Atomic Layer Deposition of Vanadium Oxide as Hole-Selective Contact for Crystalline Silicon Solar Cells

DOI: 10.1002/ ((please add manuscript number))
Article type: Full Paper

Atomic Layer Deposition of Vanadium Oxide as Hole-Selective Contact for Crystalline Silicon Solar Cells

Xinbo Yang, Hang Xu, Wenzhu Liu, Qunyu Bi, Lujia Xu, Jingxuan Kang, Mohamed N. Hedhili, Baoquan Sun, Xiaohong Zhang, Stefaan De Wolf**

Prof. Dr. Xinbo Yang
College of Energy, Soochow Institute for Energy and Materials InnovationS (SIEMIS), Soochow University, Suzhou 215006, PR China
E-mail: xbyang0205@suda.edu.cn

Dr. Xinbo Yang, Hang Xu, Dr. Wenzhu Liu, Dr. Qunyu Bi, Dr. Lujia Xu, Jingxuan Kang, Prof. Dr. Stefaan De Wolf
KAUST Solar Center, King Abdullah University of Science and Technology (KAUST), Thuwal 23955-6900, Saudi Arabia
E-mail: xinbo.yang@kaust.edu.sa (X. Yang); stefaan.dewolf@kaust.edu.sa (S. De Wolf)

Prof. Dr. Baoquan Sun, Prof. Dr. Xiaohong Zhang
Institute of Functional Nano & Soft Materials (FUNSOM), Jiangsu Key Laboratory for Carbon-Based Functional Materials & Devices, Collaborative Innovation Center of Suzhou Nano Science & Technology, Soochow University, 199 Ren'ai Road, Suzhou, 215123, Jiangsu, PR China

Dr. Mohamed N. Hedhili
KAUST Core Lab, King Abdullah University of Science and Technology (KAUST), Thuwal 23955-6900, Saudi Arabia

Keywords: passivating contact; carrier selective contact; vanadium oxide; silicon solar cell

ABSTRACT

High carrier recombination losses at the contact regions has become the dominant factor limiting the power conversion efficiency (PCE) of crystalline silicon (*c*-Si) solar cells. Dopant-free carrier-selective contacts are being intensively developed to overcome this challenge. In this work, vanadium oxide (VO_x) deposited by atomic layer deposition (ALD) is investigated and optimized as a potential hole-selective contact for *c*-Si solar cells. ALD VO_x films are demonstrated to simultaneously offer a good surface passivation and an acceptable contact resistivity (ρ_c) on *c*-Si, achieving a best contact recombination current density (J_0) of ~ 40 fA/cm^2 and a minimum ρ_c of ~ 95 mΩ.cm^2. Combined with a high work function of 6.0 eV, ALD VO_x films are proven to be an effective hole-selective contact on *c*-Si. By the implementation of hole-selective VO_x contact, we demonstrate the state-of-the-art PCE of 21.6% on *n*-type *c*-Si solar cells with a high stability. These results demonstrate the high potential of ALD VO_x as a stable hole-transport layer for photovoltaic devices, with applications beyond *c*-Si, such as perovskite and organic solar cells.

1. Introduction

The current photovoltaic (PV) market is dominated by the wafer-based *c*-Si PV technology, occupying a very high market share of ~95%,[1] thanks to its low-cost, long stability, availability, nontoxicity, and well-developed processing techniques. In China, the dominant *c*-Si PV manufacturer and the biggest PV market, without subsidies, hundreds of cities can nowadays achieve solar PV electricity prices lower than grid-supplied prices.[2] Currently most of the commercial *c*-Si PV modules consist of so-called Al-BSF (aluminum back surface field) or PERC (passivated emitter and rear cell) cells, both featuring direct metal contacts on the *c*-Si absorber with either phosphorus or boron doping by high temperature diffusion. The PCEs of Al-BSF and PERC cells are significantly limited by the high carrier recombination losses at the metal-silicon contact regions (up to 50%), due to a high density of active states at the contact interface that lie within the silicon bandgap.[3,4] Moreover, heavy doping by high temperature diffusion also induces Auger recombination, bandgap narrowing and free carrier absorption, which further limit the PCE of *c*-Si solar cells.[5]

To enhance the *c*-Si solar cell performance, carrier-selective contacts (CSCs) are being developed to replace the doped p-n junctions and mitigate their associated deleterious effects. High quality CSCs effectively passivate the whole *c*-Si surface and selectively collect one type of charge carrier (*e.g.* the electrons), while blocking the opposite type (*e.g.* the holes). In this way, CSC technology eliminates conventional diffused doping processes and significantly reduces carrier recombination in both the contact and non-contact regions, yielding an open circuit voltage (V_{oc}) close to the theoretical limit. Simultaneously, CSCs also offer suitably low contact resistivity (ρ_c) and one-dimensional carrier extraction, enabling a high fill factor (*FF*), as well as a low process complexity without contact patterning. Indeed, recent years have seen that all of the *c*-Si solar cells

with PCEs higher than 25% feature carrier-selective contacts on either one polarity or both polarities of the device.[5] Successful examples of CSCs are doped silicon layer based silicon heterojunction (SHJ) and poly-Si passivating contact technologies, consisting of a stack of hydrogenated amorphous silicon (a-Si:H)/doped a-Si:H and SiO_x/doped poly-Si, respectively.[5,6] By implementation of high quality SHJ and poly-Si passivating contact technologies, outstanding PCEs of 26.7% and 26.1% have been achieved for *c*-Si solar cells, respectively, both record devices featuring an interdigitated back contact (IBC) architecture.[7,8] However, doped silicon layer based CSCs suffer from optical losses due to the parasitic absorption, and the deposition process involves toxic and flammable gases (*e.g.*, silane, phosphine) with mandatory safety control.

Alternatively, thin films (*e.g.* metal oxides, nitrides and fluorides) with extremely low or high work function (φ) and/or suitable band alignment with *c*-Si have also been intensively investigated as so-called dopant-free CSCs for *c*-Si solar cells.[9-30] For example, TiO_2, TaO_x, NdO_x, TaN_x and TiN films featuring a small conduction band offset (ΔE_c) with *c*-Si, and LiF, MgF_2, Ca and Mg featuring a low work function were developed as electron-selective contacts (ESCs).[9-21] Similarly, thin films with a high work function (*e.g.* MoO_x, VO_x and WO_x) or a small valance band offset (ΔE_v) with *c*-Si (*e.g.* NiO_x, PEDOT:PSS) were investigated as hole-selective contacts (HSCs).[22-30] These dopant-free CSCs are easy to deposit at a low temperature using thermal evaporation, sputtering, and atomic layer deposition (ALD). The most successful dopant-free CSCs so far are electron-selective TiO_2 and hole-selective MoO_x contacts, achieving a high PCE of 22.1% and 23.5%, respectively, using a full-area contact architecture.[15,23] Recently, by integrating the electron-selective ZnO/LiF and hole-selective MoO_x contacts, an impressive PCE of 21.4% was achieved on a fully dopant-free *c*-Si solar cell without diffused p-n junctions.[31] All these achievements have demonstrated the high potential of dopant-free CSCs for *c*-Si solar cells.

Development of high quality HSCs is challenging, and MoO_x is the most successful example, thanks to its ease of deposition by thermal evaporation and high performance on devices. MoO_x films deposited by ALD were also investigated; however, the results indicated that the work function of ALD MoO_x may be too low to be an efficient HSC on *c*-Si devices.[32,33] VO_x films deposited by thermal evaporation were also intensively investigated as potential HSC, and Gerling *et al.* demonstrated that VO_x is superior to MoO_x in terms of surface passivation, which predicts the high potential of VO_x as HSC on *c*-Si solar cells.[24-26] However, until now the best PCE of *c*-Si solar cell with VO_x contact only reaches 19.7%.[26] In this work, we present a high performance VO_x HSC deposited by ALD. The surface passivation, hole-selectivity, and stability of ALD VO_x were investigated thoroughly. Contrasting to ALD MoO_x, VO_x films deposited by ALD are proven to be efficient as HSC for *c*-Si solar cells, featuring a high work function, a good surface passivation and an acceptable ρ_c simultaneously. By implementation of the optimal hole-selective VO_x contact, a remarkable PCE of 21.6% is achieved on an n-type *c*-Si solar cell.

2. Results and Discussion

Since a high work function has been proven to be the basic prerequisite for achieving a high quality hole-selectivity,[25,26] we optimize the VO_x film deposition recipes based on the work functions extracted from ultraviolet photoelectron spectroscopy (UPS) data. Three different deposition temperatures (160, 200 and 230°C) were chosen, considering the thermal stability of a-Si:H passivation interlayer (≤ 250°C) and final curing temperature for the device (~ 200°C). Figure 1a shows the UPS spectrum of VO_x films deposited at different temperatures, using a He I excitation (21.22 eV) after surface etching with Ar^{3+} ions. The work function and the difference between the Fermi level and the maximum of valence band ($E_f - E_v$), shown as inset in Figure 1a, are determined from the onset at high binding energy and the cutoff at low binding energy in the

UPS spectrum, respectively. We observe that the work function of VO_x film increases with increasing deposition temperature, and a high work function of ~ 6.0 eV is achieved on VO_x film deposited at 230°C. This value is lower than the reported φ of ~ 6.8 eV measured on polycrystalline V_2O_5 film,[34] which might be attributed to an oxygen deficiency in the amorphous ALD VO_x film (see the TEM image in Figure 3). Fortunately, it is greater than the valence band energy of intrinsic a-Si:H (~ 5.62 eV), which is essential for efficient hole transport when combined with a-Si:H passivation interlayer, by inducing a high upward band bending and forming an induced *p-n* junction at *c*-Si surface, similar as for MoO_x-based SHJ cells.[22] The sub-bandgap defect band observed between the valence band and Fermi energy can be attributed to surface etching damage, because no sub-bandgap defect band is observed before surface etching (see Supplementary Figure S1). The $E_f - E_v$ values are determined to be 3.0 ± 0.1 eV, and the optical bandgap of the VO_x film is ~ 2.9 eV, obtained from spectroscopic ellipsometry. The result indicates that the Fermi level is quite close to the conduction band minimum, demonstrating that ALD VO_x is a highly n-type material, as a result of high oxygen vacancies. Unless stated otherwise, the VO_x film discussed here is deposited at 230°C. Figure 1b shows the high-resolution X-ray photoelectron spectroscopy (XPS) core-level spectra of V 2p and O 1s for the VO_x film. The V 2p core level consists of two doublets V $2p_{3/2}$ – V $2p_{1/2}$ with a fixed area ratio of 2:1. The binding energies of V $2p_{3/2}$ is fitted by a dominant peak at 517.4 eV (red) and a small shoulder at 516.3 eV (blue), which can be attributed to V^{5+} and V^{4+} oxidation states, respectively.[35-36] The atomic ratio of V^{5+} and V^{4+} is determined to be ~ 8.4, indicating that as-grown VO_x film is dominated by the V_2O_5 phase and oxygen deficient. The optical bandgap of the VO_x film (~ 2.9 eV) also confirms this phase (VO_2 has a low bandgap of ~ 0.6 eV).[37] The O 1s core level is fitted by two components located at 530.6 and 531.8 eV, corresponding to vanadium oxide and hydroxide, hydrated oxygen and

defective oxygen, respectively.[38,39] In summary, XPS and UPS measurements demonstrate that by ALD we obtained oxygen-deficient VO_x films with a high work function, exhibiting good characteristics to be a promising HSC on *c*-Si solar cells.

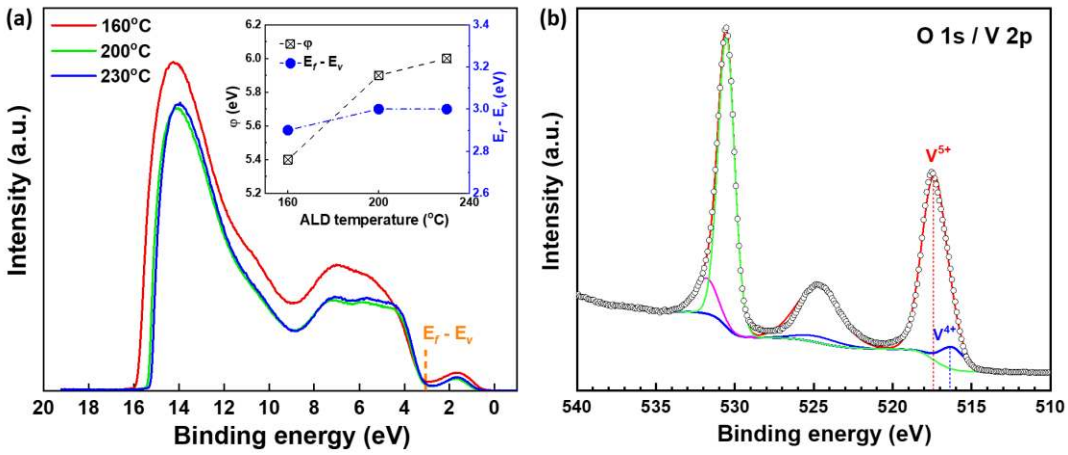

Figure 1. (a) UPS spectrum of ALD VO_x films deposited at different temperatures, and the extracted work function and $E_f - E_v$ as a function of deposition temperature are shown as inset. (b) XPS core-level spectra of V 2p and O 1s of VO_x film deposited at 230°C.

In the following sections, the most important properties of VO_x on *c*-Si from a device perspective, the carrier recombination parameter (J_0) and ρ_c, are investigated. Figure 2a and 2c show the injection level dependent effective carrier lifetimes (τ_{eff}) of *n*-type and *p*-type *c*-Si substrates (*n*-Si, 1.5 Ω·cm and *p*-Si, 4.5 Ω·cm) passivated by VO_x films with different thickness, respectively. The corresponding J_0 and implied open circuit voltage (i-V_{oc}) as a function of VO_x thickness are displayed in Figure 2b and 2d. Thin VO_x films exhibit good surface passivation on both *n*- and *p*-Si, featuring an increased τ_{eff} and i-V_{oc} with increasing VO_x thickness. As the VO_x film thickness increases from 4.0 to 9.0 nm, the measured τ_{eff} (at the minority carrier density of 1×10^{15} cm^{-3}) increases from 290 to 670 µs on *n*-Si, corresponding to a decreased J_0 from 95 to 40 fA/cm^2 and an increased i-V_{oc} from 650 to 674 mV. Further increasing the VO_x thickness to 12.0 nm results in a slightly reduced τ_{eff} (645 µs) and i-V_{oc} (672 mV). A quite similar trend is observed

on VO_x passivated *p*-Si, and a lowest J_0 of 44 fA/cm^2 and a highest i-V_{oc} of 672 mV is obtained with 9.0 nm VO_x. The best J_0 obtained by ALD VO_x is much lower than that of thermal evaporated VO_x (175 ± 10 fA/cm^2) and MoO_x (~ 300 fA/cm^2).[25,40] Moreover, the τ_{eff} of ALD VO_x passivated samples exhibit slight degradation after exposure in the air ambient for few days (see Supplementary Figure S2), indicating good environmental stability and the high work function can be maintained during device fabrication. In contrast, Masmitja *et al.* observed a significant τ_{eff} degradation with time on thermally-evaporated VO_x passivated *c*-Si, which can be attributed to the work function reduction of VO_x due to the chemical reactions in the air.[25] Interestingly, the thermal stability of ALD VO_x passivation on *c*-Si is similar to that of thermal evaporated VO_x (up to ~300°C, see Supplementary Figure S3),[25] demonstrating a high compatibility with the contemporary metallization techniques of SHJ solar cells (*e.g.* screen-printing Ag paste curing at ~ 200°C).

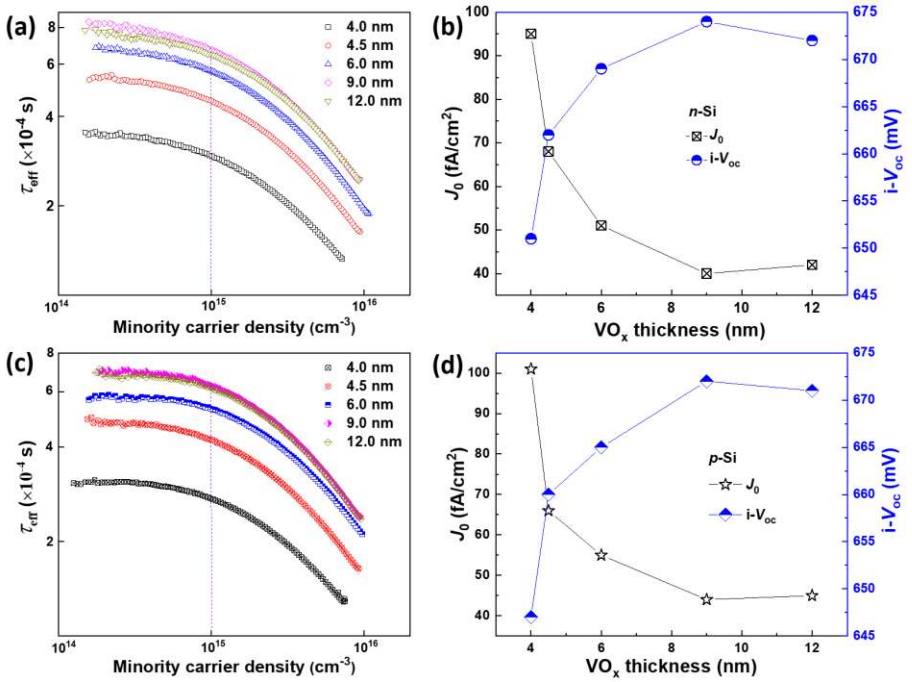

Figure 2. Injection level dependent τ_{eff} of (a) *n*-Si and (c) *p*-Si passivated by VO_x films with different thickness; Dependence of J_0 and i-V_{oc} of (b) *n*-Si and (d) *p*-Si on the VO_x film thickness.

To unveil the passivation mechanism of VO_x on *c*-Si, contactless capacitance-voltage (C-V) measurements were conducted. Unfortunately, VO_x films were found to be quite leaky, and we failed to quantify of the fixed charge density (Q_f) and interface defect density (D_{it}). This might be attributed to the high work function of VO_x, which induces strong band bending and an inversion layer on *n*-Si surface. We suspect that the high current leakage during C-V measurement might be the characteristic of dopant-free CSCs, which was also observed in electron-selective TiO_2 contact on *c*-Si.[41] Figure 3a shows the cross-sectional high-resolution transmission electron microscopy (HRTEM) image of the VO_x/*c*-Si interface, in which a thin interlayer (~ 2.0 nm) between VO_x and *c*-Si is clearly observed. The VO_x/*c*-Si interface is further analysed using high angle annular dark field (HAADF) scanning TEM coupled with energy dispersive X-ray spectroscopy (EDX) to confirm the composition of these layers, as shown in Figure 3b. The EDX element mapping confirms the presence of a SiO_x interlayer between VO_x and *c*-Si interface, which was also observed at the thermal-evaporated VO_x/*c*-Si interface.[25] Therefore, the passivation mechanism of VO_x on *c*-Si can be regarded as the combination of chemical passivation of SiO_x and field-effect passivation of the VO_x film. The field-effect passivation of the VO_x film is also proven when capping on a-Si:H passivation interlayer, resulting in an increased τ_{eff} from ~ 7.1 ms (5.0 nm a-Si:H only) to ~ 15.5 ms with 4.5 nm VO_x capping layer (see Supplementary Figure S4).

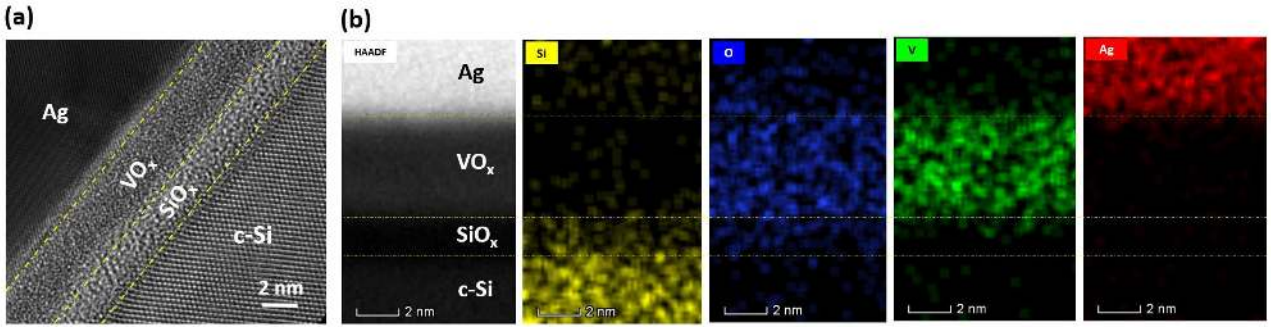

Figure 3. (a) Cross-sectional HRTEM image of *c*-Si/VO_x interface; (b) HAADF STEM and EDX element mappings of the Si, V, O and Ag concentrations at *c*-Si/VO_x/Ag interfaces.

Next we investigate the ρ_c of the VO_x/*c*-Si heterocontact using Cox and Strack method.[42] This method involves a series of resistance measurements on a test structure with different diameter circular contacts (inset in Figure 4a); ρ_c values were then extracted by fitting the curve of resistance versus contact diameter, as detailed in the previous reports.[13,15,21,40] Figure 4a shows the dependence of ρ_c of the VO_x/*p*-Si and VO_x/a-Si:H/*p*-Si heterocontacts on VO_x thickness. With increasing VO_x thickness from 4.5 to 12 nm, ρ_c increases from 95 to 177 mΩ.cm^2. The minimum ρ_c of VO_x/*c*-Si heterocontact is similar to that of thermal evaporated VO_x on *c*-Si measured by transmission-line-method (TLM),[43] but much higher than that of thermal-evaporated MoO_x on *c*-Si (~ 1.0 mΩ.cm^2).[40] It might be ascribed to the presence of a thick SiO_x interlayer in the VO_x contact (shown in Figure 3a) as well as the different measurement structure, where a high work function palladium electrode was used in MoO_x contact measurement.[40] When an intrinsic a-Si:H passivation interlayer (5 nm) is inserted, the ρ_c increases significantly with increasing VO_x thickness. The minimum ρ_c of 104 mΩ.cm^2 is obtained with the thinnest VO_x (4.5 nm), comparable to that of the best reported a-Si:H/a-Si:H(p) contact (~ 100 mΩ.cm^2) in conventional SHJ device.[44] Note that the ρ_c extracted here should be considered as the upper limit value for the VO_x/*p*-Si and VO_x/a-Si:H/*p*-Si heterocontacts, because it consists of the resistance of the front VO_x/*p*-Si and rear *p*-Si/Al interfaces, as well as the bulk resistivity of VO_x and a-Si:H. Therefore, these ρ_c values should meet the threshold ($\leq$ 100 mΩ.cm^2) for a full-area contact required to make high efficiency *c*-Si solar cells.[45] Figure 4b shows the dependence of the ρ_c of the VO_x/*p*-Si heterocontacts on temperature, which was measured on a probe station with an integrated heating system. At typical outdoor operating temperature of *c*-Si solar cells (20 - 80°C), the ρ_c of the VO_x/*p*-Si heterocontact displays a significant temperature dependence, rapidly decreases with increasing temperature. This indicates that the carrier transport at the VO_x/*p*-Si heterocontacts is dominated by thermionic

emission (TE) over the *Schottky* barrier, instead of tunneling from the SiO_x interlayer.[46] Although the thickness of the SiO_x interlayer is very close to the tunneling limit (< 2.0 nm), it is believed to be conductive because of its oxygen deficient nature, resulting in a high defect states density within the bandgap.[24] The thermionic barrier might be attributed to the misaligned band offset at the VO_x/*p*-Si interface, however, further work is needed to unveil the mechanism.

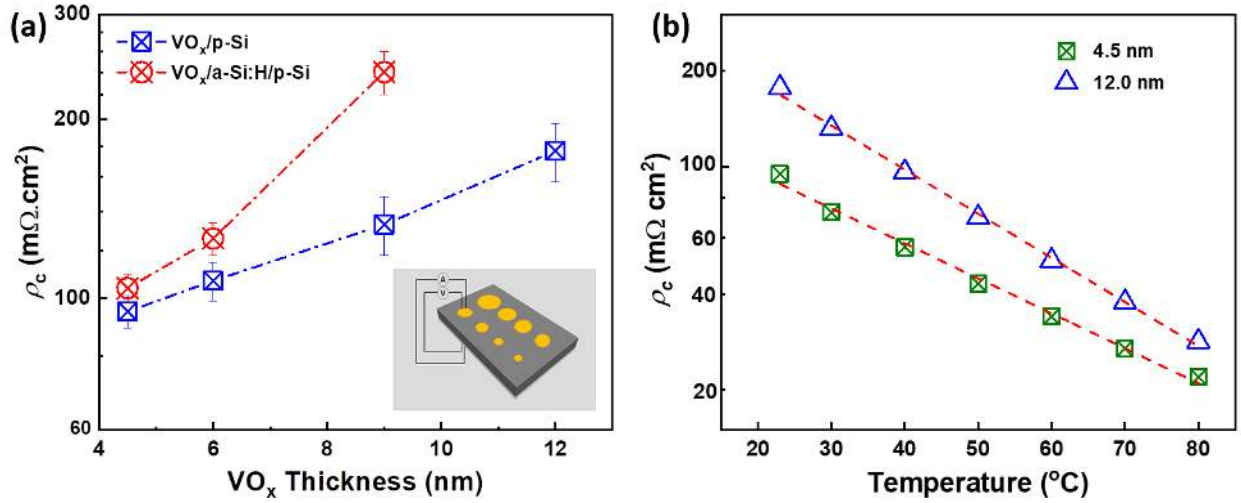

Figure 4. (a) Dependence of ρ_c of VO_x/*p*-Si and VO_x/a-Si:H/*p*-Si heterocontacts on VO_x thickness; (b) ρ_c of VO_x/*p*-Si heterocontact as a function of temperature.

After optimizing the hole-selective VO_x contact, we verify its functioning on a device featuring a rear-junction SHJ architecture, sketched in Figure 5a. A thin VO_x film (~ 4.5 nm) is utilized at the rear to replace the standard boron-doped a-Si: H for hole extraction. The electron extraction layer at the front consists of a stack of an intrinsic a-Si: H passivation layer and phosphorus-doped a-Si:H (n^+ a-Si: H), capped with indium doped tin oxide (ITO). Figure 5b shows the light *J*-*V* curve of the best device (2×2 cm^2) with VO_x contact, featuring a high V_{oc} of 721 mV, a J_{sc} of 38.3 mA/cm^2, a *FF* of 78.2%, resulting in a high PCE of 21.6%. To the best of our knowledge, this is the highest PCE reported on *c*-Si solar cell with hole-selective VO_x contact. The *pseudo* device before metallization exhibits a very high τ_{eff} of ~ 9.5 ms and a high i-V_{oc} of 729 mV (see

Supplementary Figure S5), indicating excellent surface passivation on both sides. The PCE is mainly limited by a moderate *FF*, due to a high series resistance of 1.03 Ω.cm^2. The J_{sc} is reasonable for a SHJ device, suffering from parasitic absorption of intrinsic and doped a-Si:H of the front layers. Figure 5c displays the statistical distribution of the photovoltaic parameters of 14 devices from the same batch. An average PCE of 21.4% is achieved, demonstrating the high manufacturability of *c*-Si solar cells with hole-selective VO_x contact. The external quantum efficiency (EQE), reflection (R) and the internal quantum efficiency (IQE) of the best device are shown in Figure 5d. The device exhibits an excellent QE at the near infrared wavelength range, indicating very low carrier recombination loss at the rear VO_x contact. The J_{sc} of the device calculated by integrating the EQE and the air mass (AM) 1.5 G product is 39.9 mA/cm^2, in good agreement with the measured J_{sc} value after considering the grid shading (~ 4.0%). After exposure in the ambient air for 3 months, the best device exhibits a negligible efficiency degradation from 21.6 to 21.5% (see Supplementary Table S1), demonstrating a high environmental stability of *c*-Si solar cells with VO_x contact.

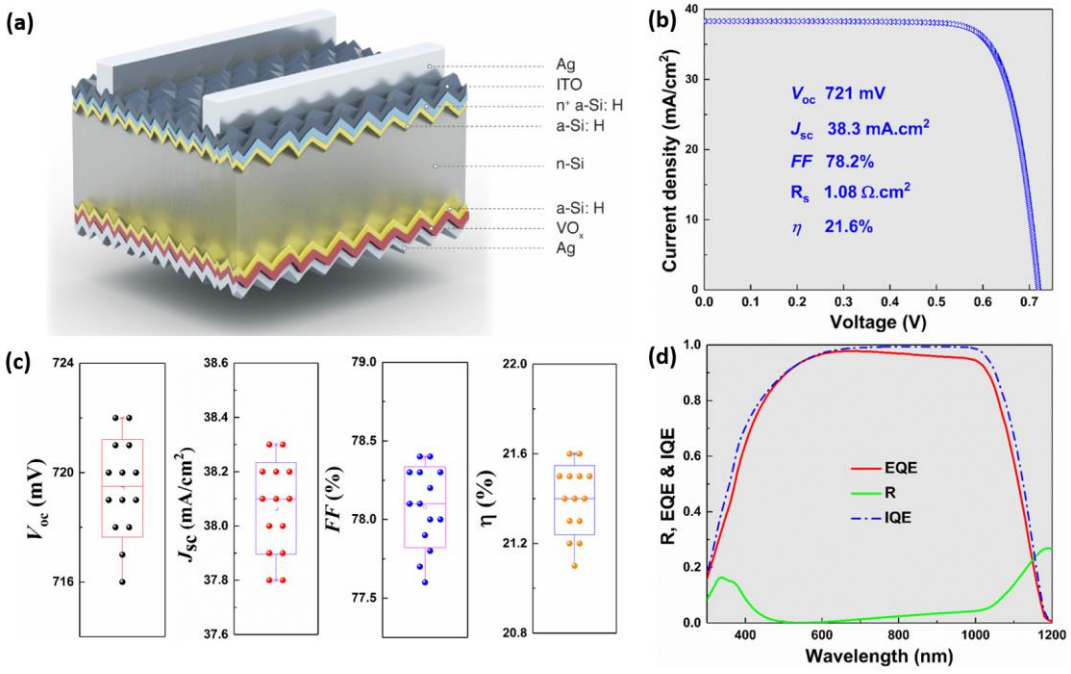

Figure 5. (a) The sketch and (b) light *J-V* curve of *n*-Si solar cell with hole-selective VO_x rear contact; (c) Statistical distribution of the photovoltaic parameters of 14 devices with hole-selective VO_x contact; (d) EQE, R and IQE of the best *n*-Si solar cell with hole-selective VO_x contact.

To further improve the device performance, we analyze the power and optical losses of the 21.6% efficiency device. Firstly, the power losses are analyzed by simulating the device with a free available software, Quokka, featuring an integrated free energy loss analysis (FELA) function.[47] The main input parameters for the simulation are listed in Supplementary Table S2. Please note that some of the key parameters were obtained from the experiments, e.g., J_0 and ρ_c at the front and rear sides, the series and shunt resistances. The unit cell generated by Quokka and the simulated *J-V* curve are shown in Supplementary Figure S6. As can be seen, the simulated photovoltaic parameters (V_{oc} 721 mV, J_{sc} 38.3 mA/cm^2, *FF* 78.2%) exhibits excellent agreement with the measured values shown in Figure 5b, indicating the high accuracy of the device model. Based on the obtained FELA data, the power losses distribution of the device is shown in Figure 6a. We can see that the resistance and recombination losses from rear VO_x contact only contribute to a small fraction of power losses (10%), thanks to an excellent surface passivation ($J_0 \sim 5$ fA/cm^2) and a moderate ρ_c for a full-area contact. Series resistance and bulk recombination in the high quality float-zone silicon substrate are identified as the two dominant factors, occupying 76% of the power losses. Since the measured ρ_c of the front electron-selective contact (~ 50 mΩ.cm^2) and rear a-Si:H/VO_x contact (~ 100 mΩ.cm^2) are acceptable for a full-area contact design, we suspect that the high series resistance of the device is most probably caused by a moderate quality screen-printed front silver contact and the shading effect on front ITO using a shadow mask, resulting in a thinner ITO with a higher sheet resistance at the edges. The high bulk recombination loss (mainly Auger recombination) might be

attributed to a thick n-type silicon substrate (~ 200 μm), which limits the V_{oc}. Silicon wafers with a typical thickness of 130 ~ 150 μm is commonly used in our SHJ baseline, achieving a maximum V_{oc} of ~ 744 mV. Therefore, next step for V_{oc} and *FF* improvement is to reduce the series resistance by optimizing the screen-printing recipe and mask design, and to use a thinner silicon wafer.

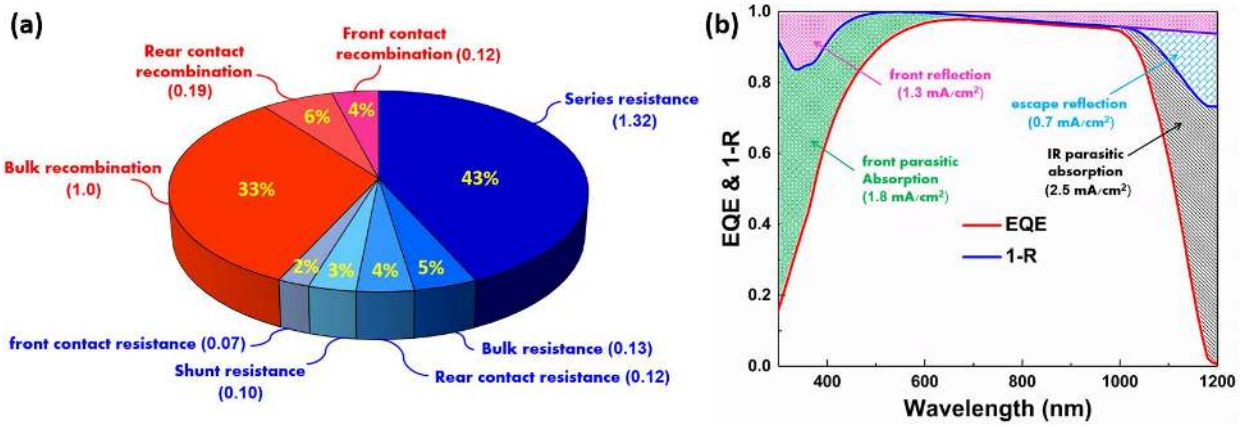

Figure 6. (a) Power losses and (b) optical losses analysis of the best *c*-Si solar cell with hole-selective VO_x contact, based on the FELA results from Quokka simulation, and EQE and 1-R data, respectively.

The optical losses of the best device is analyzed using the EQE and 1-R data, as proposed by Holman *et al.*[48] The current losses from different parts are calculated by integrating over photon flux density of AM 1.5G, and the result is shown in Figure 6b. We identify that the parasitic absorption losses at front (1.8 mA/cm²) and rear (2.5 mA/cm²) sides dominate the current losses, which can be mainly attributed to the parasitic absorption from intrinsic and doped a-Si:H, and front ITO as well. Considering the highly transparent of ALD VO_x (see Supplementary Figure S7), the front parasitic absorption loss may be improved by using the wide bandgap VO_x as the window layer. The high current loss at the rear side might be caused by a poor reflection, due to the lack of rear ITO and a non-mirror Ag rear electrode. To reduce the current losses of the device, it is essential to confirm that the hole-selectivity of VO_x can

be maintained after capping with transparency conductive oxide (TCO). It is an open topics for future investigation.

3. Conclusions

We have successfully developed a high quality hole-selective, passivating contact for *c*-Si solar cells. VO_x films deposited by ALD are optimized to be an efficient hole-selective contact, simultaneously featuring a high work function (6.0 eV), a good surface passivation (best $J_0 \sim 40$ fA/cm^2) and an acceptable ρ_c (minimum ~95 mΩ.cm^2) on *c*-Si. The ALD VO_x offers an excellent hole-selectivity with better environmental stability, resulting in a state-of-the-art efficiency of 21.6% on *c*-Si solar cell featuring a full-area VO_x passivating contact. The high work function VO_x with a better stability might also be interesting for perovskite and organic solar cells.

Experimental section

VO_x film deposition and characterization: VO_x films were deposited at different temperatures (160, 200 and 230 °C) by thermal ALD, using vanadyl tri-isopropoxide (VTIP) as the vanadium precursor and deionized water as the oxidant. To prevent precursor condensation, VTIP bubbler and tube lines were heated to 50°C and 60°C, respectively. A continuous flow of argon (Ar) was used as the purge and carrier gas throughout the deposition process. One VO_x growth cycle consists of a VTIP pulse for 2.0 s, an Ar purge for 4.0 s, a H_2O pulse for 0.5 s and an Ar purge for 4.0 s, resulting in a growth rate of ~ 0.4 nm/cycle at 230°C (see Supplementary Figure S8). The thicknesses and optical bandgap of VO_x films were determined by Ellipsometer (M-2000, J. A. Woollam). The work function of the VO_x films were measured by UPS (Kratos Axis Ultra) using a He-I excitation (21.22 eV) after surface etching with Ar^+ ions. The chemical bonding states of VO_x films were determined by high-resolution XPS (Kratos Axis, Kratos Analytical Ltd.) equipped with a monochromatic Al Kα x-ray source (1486.6 eV). High-resolution spectra were performed at fixed analyzer pass energies of 160 eV and 20 eV, and quantified using empirically derived relative sensitivity factors provided by the manufacturer. Binding energies were calibrated using the C 1s peak, which was set at 285.0 eV. XPS spectra were analyzed using CasaXPS, a commercially available software.

The passivation quality of VO_x films on *c*-Si was evaluated using the quasi-steady state photoconductance (QSSPC) technique.[49] VO_x films with the same thickness were deposited on

both sides of *n*-Si (1.5 Ω·cm) and *p*-Si (4.5 Ω·cm) wafers, preparing a symmetrical test structure for τ_{eff} and i-V_{oc} measurements on a Sinton lifetime tester (WCT-120, Sinton Instruments). The J_0 values were extracted from the measured τ_{eff} using the Kane and Swanson method.[50] The thermal stability of VO_x on *c*-Si was investigated by measuring the τ_{eff} before and after annealing in a tube furnace at different temperatures under N_2 atmosphere. The ρ_c of the VO_x/*c*-Si heterocontacts were measured using Cox and Strack method.[42] The test structures, shown as inset in Figure 4a, were prepared by depositing different thickness VO_x on the front side of *p*-Si (0.1 Ω·cm), following which Ag circular contacts (300 nm) with different diameters were evaporated through a shadow mask. The rear side figures a full-area Al contact (500 nm), exhibiting ohmic contact on the heavily doped *p*-Si. Dark *J*-*V* measurements were performed on a probe station with heating function, and ρ_c values were extracted by fitting the trend of resistance versus diameter of the front contacts. HRTEM and STEM coupled with EDX characterizations of the VO_x/*c*-Si interface were carried out using a Titan 80-300 ST TEM (FEI Company) operated at an accelerating voltage of 300 kV. HRTEM image was acquired using an Ultra-Scan CCD camera from Gatan Inc.

Device fabrication and characterization: Silicon solar cells (2 × 2 cm^2) with a hole-selective VO_x rear contact were fabricated on high quality float-zone *n*-Si wafers (1.0 Ω·cm, ~ 200 μm). After both-side texturing with random pyramids in a KOH solution and experiencing a standard RCA cleaning, a stack of intrinsic and phosphorus-doped a-Si: H (5/5 nm) was deposited on the front side continuously without vacuum break. An ITO layer (~ 75 nm) was capped by sputtering through a shadow mask, defining the active cell area at the front. Then an intrinsic a-Si: H passivation layer (~ 5 nm) was deposited on the rear side, following by a thermal annealing at 250°C in the air for 20 mins in a tube furnace, as suggested by Essig *et al.*[51] All the a-Si: H layers were deposited in a multi-chamber, plasma enhanced chemical vapor deposition (PECVD) system

at 200°C. After removing the rear surface oxide by a short HF dip, the samples were transferred into the ALD chamber for VO_x deposition immediately, and then metallized with a thermally evaporated Ag electrode (1000 nm). The front Ag fingers were finally prepared by screen-printing using a low-temperature Ag paste and curing at 190°C for 20 mins in the air.

The light *J-V* characteristics of the devices were measured using a light emitter diode (LED)-based solar simulator under standard test conditions (25°C, 1000 W/m^2, AM1.5). The light intensity was calibrated with a reference cell prepared by Frauhofer ISE CalLab. The EQE and reflection of the devices were characterized by the solar cell analysis system LOANA (pv-tools, GmbH), which include an EQE measurement setup that provides monochromatic light between 280-1600 nm. The simulation software, Quokka 2, was downloaded from *PV lighthouse*.

Supporting Information

Supporting Information is available from the Wiley Online Library or from the author.

Acknowledgements

The work presented in this publication was financially supported by King Abdullah University of Science & Technology (KAUST), through the Competitive Research Grant. B. S. and X. Z. acknowledge the National Natural Science Foundation of China (No. 91833303). We would like to thank Dr. Michele De Bastiani and Dr. Thomas Allen in KAUST for helping the device fabrication and Dr. Ziv Hameiri (University of New South Wales) for conducting the contactless capacitance-voltage (*C*-*V*) measurements. We also thank Heno Hwang, scientific illustrator at KAUST, for producing Figure 5(a).

References

[1] Fraunhofer Institute for Solar Energy Systems, *Photovoltaics Report*, March 2019.

[2] J. Yan, Y. Yang, P. E. Campana, J. He, *Nature Energy* **2019**, 4, 709.

[3] J. Benick, B. Hoex, M. Sanden, W. Kessels, O. Schultz, S. Glunz, *Appl. Phys. Lett.* **2008**, 92, 253504.

[4] M. Sajjad, X. Yang, P. Altermatt, N. Singh, U. Schwingenschlögl, S. De Wolf, *Appl. Phys. Lett.* **2019**, 114, 071601.

[5] T. Allen, J. Bullock, X. Yang, A. Javay, S. De Wolf, *Nature Energy* **2019**, 4, 914.

[6] J. Schmidt, R. Peibst, R. Brendel, *Sol. Energy Mater. Sol. Cells* **2018**, 187, 39.

[7] K. Yoshikawa, W. Yoshida, T. Irie, H. Kawasaki, K. Konishi, H. Ishibashi, T. Asatani, D. Adachi, M. Kanematsu, H. Uzu, K. Yamamoto, *Sol. Energy Mater. Sol. Cells* **2017***,* 173, 37.

[8] F. Haase, C. Hollemann, S. Schäfer, A. Merkle, M. Rienäcker, J. Krügener, R. Brendel, R. Peibst, *Sol. Energy Mater. Sol. Cells* **2018**, 186, 184.

[9] Y. Zhang, R. Liu, S. Lee, B. Sun, *Appl. Phys. Lett.* **2014**, 104, 083514.

[10] Y. Zhang, W. Cui, Y. Zhu, F. Zu, L. Liao, S. Lee, B. Sun, *Energy Environ. Sci* **2015**, 8, 297.

[11] X. Yang, P. Zheng, Q. Bi, K. Weber, *Sol. Energy Mater. Sol. Cells* **2016**, 150, 32.

[12] Y. Wan, C. Samundsett, J. Bullock, T. Allen, M. Hettick, D. Yan, P. Zheng, X. Zhan, J. Cui, J. McKeon, A. Javey, A. Cuevas, *ACS Appl. Mater. Interface.* **2016**, 8, 14671.

[13] X. Yang, Q. Bi, H. Ali, K. Davis, W. Schoenfeld, K. Weber, *Adv. Mater.* **2016**, 28, 5891.

[14] J. Bullock, M. Hettick, J. Geissbühler, A. Ong, T. Allen, C. Sutter-Fella, T. Chen, H. Ota, E. Schaler, S. De Wolf, C. Ballif, A. Cuevas, A. Javey, *Nat. Energy* **2016**, 1, 15031.

[15] X. Yang, K. Weber, Z. Hameiri, S. De Wolf, *Prog. Photovolt.* **2017**, 25, 896.

[16] T. Allen, J. Bullock, P. Zheng, B. Vaughan, M. Barr, Y. Wan, C. Samundsett, D. Walter, A. Javey, A. Cuevas, *Prog. Photovolt.* **2017**, 25, 636.

[17] B. Macco, L. E. Black, J. Melskens, B. Loo, W. H. Berghuis, M. Verheijen, W. Kessels, *Sol. Energy Mater. Sol. Cells* **2018**, 184, 98.

[18] X. Yang, E. Aydin, H. Xu, J. Kang, M. Hedhili, W. Liu, Y. Wan, J. Peng, C. Samundsett, A. Cuevas, S. De Wolf *Adv. Energy Mater.* **2018**, 8, 1800608.

[19] Y. Wan, S. Karuturi, C. Samundsett, J. Bullock, M. Hettick, D. Yan, J. Peng, P. Narangari, S. Mokkapati, H. Tan, C. Jagadish, A. Javey, A. Cuevas, *ACS Energy Lett.* **2018**, 3, 125.

[20] H. Tong, Z. Yang, X. Wang, Z. Liu, Z. Chen, X. Ke, M. Sui, J. Tang, T. Yu, Z. Ge, Y. Zeng, P. Gao, J. Ye, *Adv. Energy Mater.* **2018**, 8, 1702921.

[21] X. Yang, W. Liu, M. De Bastiani, T. Allen, J. Kang, H. Xu, E. Aydin, L. Xu, Q. Bi, H. Dang, E. AlHabshi, K. Kotsovos, A. AlSaggaf, I. Gereige, Y. Wan, J. Peng, C. Samundsett, A. Cuevas, S. De Wolf, *Joule* **2019**, 3, 1314.

[22] C. Battaglia, X. Yin, M. Zheng, I. D. Sharp, T. Chen, S. McDonnell, A. Azcatl, C. Carraro, B. Ma, R. Maboudian, R. M. Wallace, A. Javey, *Nano Lett.* **2014**, 14, 967.

[23] J. Dreon, Q. Jeangros, J. Cattin, J. Haschke, L. Antognini, C. Ballif, M. Boccard, Nano Energy **2020**, 70, 104495.

[24] L. G. Gerling, S. Mahato, A. Morales-Vilches, G. Masmitja, P. Ortega, C. Voz, R. Alcubilla, J. Puigdollers, *Sol. Energy Mater. Sol. Cells* **2016**,145,109.

[25] G. Masmitja, L. G. Gerling, P. Ortega, J. Puigdollers, I. Martin, C. Voz, R. Alcubilla, *J. Mater. Chem. A* **2017**, 5, 9182.

[26] G. Masmitja, P. Ortega, J. Puigdollers, L. G. Gerling, I. Martin, C. Voz, R. Alcubilla, *J. Mater. Chem. A* **2018**, 6, 3977.

[27] M. Bivour, J. Temmler, H. Steinkemper, M. Hermle, *Sol. Energy Mater. Sol. Cells* **2015**, 142, 34.

[28] D. Zielke, A. Pazidis, F. Werner, J. Schmidt, *Sol. Energy Mater. Sol. Cells* **2014**, 131, 110.

[29] J. He, P. Gao, Z. Yang, J. Yu, W. Yu, Y. Zhang, J. Sheng, J. Ye, J. C. Amine, Y. Cui, *Adv. Mater.* 2017, 29, 1606321.

[30] J. He, Y. Wan, P. Gao, J. Tang, J. Ye, *Adv. Funct. Mater.* 2018, 28, 1802192.

[31] S. Zhong, J. Dreon, Q. Jeangros, E. Aydin, S. De Wolf, F. Fu, M. Boccard, C. Ballif, *Adv. Funct. Mater.* **2020**, 30, 1907840.

[32] B. Macco, M. Vos, N. Thissen, A. A. Bol, W. M. M. Kessels, *Phys. Status Solidi RRL* **2015**, 9, 393.

[33] M. Bivoura, B. Macco, J. Temmler, W. M. M. Kessels, M. Hermle, *Energy Procedia* **2016**, 92, 443.

[34] M. T. Greiner, L. Chai, M. G. Helander, W. Tang, Z. Lu, *Adv. Funct. Mater.* **2012**, 22, 4557.

[35] D. Barreca, L. Armelao, F. Caccavale, V. Noto, A. Gregori, G. Rizzi, E. Tondello, *Chem. Mater.* **2000**, 12, 98.

[36] J. Musschoot, D. Deduytsche, H. Poelman, J. Haemers, R. Meirhaeghe, S. Berghe, C. Detavernier, *J. Electrochem. Soc.* **2009**, 156, P122.

[37] G. Y. Song, C. Oh, S. Sinha, J. Son, J. Heo, *ACS Appl. Mater. Inter.* **2017**, 9, 23909.

[38] M. C. Biesinger, L. Laua, A. R. Gersonb, R. Smart, *Appl. Surf. Sci.* **2010**, 257, 887.

[39] B. P. Barbero, L. E. Cadús, L. Hilaire, *Appl. Catal. A* **2003**, 246, 237.

[40] J. Bullock, A. Cuevas, T. Allen, C. Battaglia, *Appl. Phys. Lett.* **2014**, 105, 232109.

[41] B. Liao, B. Hoex, K. D. Shetty, P. K. Basu, C. S. Bhatia, *IEEE J. Photovolt.* **2015**, 5, 1062.

[42] R. Cox, H. Strack, *Solid-State Electron.* **1967**, 10, 1213.

[43] L. G. Gerling, C. Voz, R. Alcubilla, J. Puigdollers, *J. Mater. Res.* **2016**, 32, 260.

[44] M. Leilaeioun, W. Weigand, M. Boccard, Z. J. Yu , K. Fisher, Z. C. Holman, *IEEE J. Photovolt.* **2019**, 10, 54.

[45] A. Cuevas, Y. Wan, D. Yan, C. Samundsett, T. Allen, X. Zhang, J. Cui, J. Bullock, *Sol. Energy Mater. Sol. Cells* **2018**, 184, 38.

[46] D. Schroder, D. Meier, *IEEE Trans. Elect. Devices* **1984**, 31, 637.

[47] A. Fell, *IEEE Trans. Electron Devices* **2013**, *60*, 733.

[48] Z. Holman, A. Descoeudres, L. Barraud, F. Fernandez, J. Seif, S. D. Wolf, C. Ballif, *IEEE J. Photovolt.* **2012**, 2, 7.

[49] R. Sinton, A. Cuevas, *Appl. Phys. Lett.* **1996**, 69, 2510.

[50] D. E. Kane, R. M. Swanson, Proceedings 18th IEEE Photovolt. Specialist Conf. Las Vegas, USA, **1985**, 578.

[51] S. Essig, J. Dréon, E. Rucavado, M. Mews, T. Koida, M. Boccard, J. Werner, J. Geissbuhler, P. Löper, M. Morales-Masis, L. Korte, S. De Wolf, C. Ballif. *Sol. Rapid Res. Lett.* **2018**, 2, 1700227.